ACS Catalysis

Research Article

pubs.acs.org/acscatalysis

Selective Catalytic Electroreduction of CO_2 at Silicon Nanowires (SiNWs) Photocathodes Using Non-Noble Metal-Based Manganese Carbonyl Bipyridyl Molecular Catalysts in Solution and Grafted onto SiNWs

Encarnación Torralba-Peñalver,[†] Yun Luo,[†] Jean-Daniel Compain,[‡] Sylvie Chardon-Noblat,*[,‡] and Bruno Fabre*[,†]

[†]Institut des Sciences Chimiques de Rennes (ISCR), UMR 6226 CNRS/Université de Rennes 1, Matière Condensée et Systèmes Electroactifs (MaCSE), Campus de Beaulieu, Rennes 35042 CEDEX, France

[‡]Université Grenoble Alpes/CNRS, Département de Chimie Moléculaire, UMR 5250, Laboratoire de Chimie Inorganique Redox, BP53, Grenoble 38041 CEDEX 9, France

Supporting Information

ABSTRACT: The electrocatalytic reduction of CO_2 to CO in hydroorganic medium has been investigated at illuminated (λ > 600 nm; 20 mW cm^{-2}) hydrogen-terminated silicon nanowires (SiNWs−H) photocathodes using three Mn-based carbonyl bipyridyl complexes as homogeneous molecular catalysts ([Mn(L) $(CO)_3(CH_3CN)](PF_6)$ and [Mn(bpy) $(CO)_3Br$] with L = bpy = 2,2′-bipyridine and dmbpy = 4,4′-dimethyl-2,2′-bipyridine). Systematic comparison of their cyclic voltammetry characteristics with those obtained at flat hydrogen-terminated silicon and traditional glassy carbon electrodes (GCE) enabled us to demonstrate the superior catalytic efficiency of SiNWs−H in terms of cathodic photocurrent densities and overpotentials. For example, the photocurrent densities measured at −1.0 V vs SCE for [Mn(bpy) $(CO)_3(CH_3CN)](PF_6)$ at SiNWs−H exceeded 1.0 mA cm^{-2} in CO_2-saturated CH_3CN + 5% v/v H_2O, whereas almost zero current was measured at this potential at GCE. Such characteristics have been supported by the energetic diagrams built for the different SiNWs|Mn-based catalyst interfaces. The fill factor FF and energy conversion efficiency η calculated under catalytic conditions were higher for [Mn(bpy or dmbpy) $(CO)_3(CH_3CN)](PF_6)$ (FF = 0.35 and 0.34; η = 3.0 and 2.0%, respectively). Further preparative-scale electrolysis at SiNWs−H photocathode with Mn-based complex catalysts in electrolytic solution evidenced the quantitative conversion of CO_2 to CO with a higher stability of the [Mn(dmbpy) $(CO)_3(CH_3CN)](PF_6)$ complex. Finally, in order to develop technologically viable electrocatalytic devices, the elaboration of SiNWs−H photoelectrodes modified with a Mn-based complex has been successfully achieved from an electropolymerizable catalyst, and it was shown that the electrocatalytic activity of the complex was retained after immobilization.

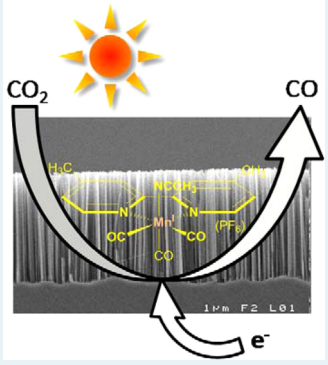

KEYWORDS: *electrocatalytic reduction of CO_2, silicon nanowires, photocathodes, Mn-carbonyl-based complexes, modified electrodes, cyclic voltammetry*

1. INTRODUCTION

With the rising atmospheric CO_2 levels, a large variety of strategies have been developed to efficiently convert this molecule to high value-added compounds.[1−7] Nevertheless, one of the main issues related to the challenge of CO_2 molecule conversion is its extreme stability. As a matter of fact, CO_2 is highly thermodynamically stable. Reactions involving CO_2 require a significant energy input concomitant to the injection of electrons and protons and necessitate the use of efficient catalysts to lower the kinetic barriers. Consequently, a large body of work has been devoted to the catalytic reduction of CO_2 and to the photoelectrochemical[8−11] and electrochemical[12−25] activation of CO_2 by using molecular catalysts to produce useful chemicals, such as carbon monoxide (CO) or formic acid (HCOOH) for instance.

In this field, the use of semiconductors (SCs) as photocathodes could provide a real benefit for the electrochemical activation of CO_2. Indeed, proton-assisted multielectron reduction potentials for CO_2 lie within the band gap of several semiconductors, such as silicon.[8] The key difference between semiconducting photoelectrodes and working electrodes traditionally used for electrocatalytic applications (e.g., metals, carbon) is that for the semiconductors, light serves as an important source of energy input. Such a property based on photovoltaic conversion can achieve an energy-saving route to electrochemical catalysis. Compared to the large number of

Received: July 21, 2015
Revised: September 10, 2015
Published: September 11, 2015

DOI: 10.1021/acscatal.5b01546
ACS Catal. 2015, 5, 6138−6147

reports devoted to the electrocatalytic reduction of CO_2 at traditional conducting electrodes, the use of SCs as photocathodes has been much less explored. As an example, Kubiak's,[8,26,27] Sato's,[28,29] and Ishitani's[30] groups have demonstrated from cyclic voltammetry experiments that the electrocatalytic potential corresponding to the reduction of CO_2 with noble metals (Re, Ru)-based carbonyl molecular catalysts in solution or attached to SC surfaces can be lowered on illuminated *p*-type Si, InP and NiO photocathodes when compared to the electroreduction on "classical" glassy carbon electrodes.

In the present work, *p*-type hydrogen-terminated silicon(100) nanowires (SiNWs−H) is used as a photocathode for the electroreduction of CO_2 in the presence of different non-noble metal (Mn)-based carbonyl bipyridyl complexes, acting as homogeneous catalysts for the reduction process. Compared with planar hydrogen-terminated silicon (Si−H), SiNWs−H can produce larger photocurrents and establish charge transfer at less-negative potentials, due to the multifaceted nature of the nanowires.[31] As a matter of fact, in an array of high-aspect-ratio nanostructures such as SiNWs, light can be absorbed effectively along the long axis of the structure. Furthermore, they are easy to prepare[32] and highly stable under reductive conditions.[33] Regarding molecular electrocatalysts, Mn non-noble-metal-based complexes, which have been first prepared and studied in our group[17,34] and since then have received careful attention from other research groups,[35−38] constitute a more sustainable approach versus the traditional one using rare and noble-metal-based species such as those containing Re, Ru, and Os.

In this work, cyclic voltammetry combined with electrochemical impedance spectroscopy, chronoamperometry measurements, and exhaustive electrolysis allow qualitative and quantitative description of the performances of the different photoelectrochemical systems studied. The CO_2 electroreduction at both planar and nanostructured silicon photocathodes was performed using various Mn-based complexes (Scheme 1). This report also includes the discussion of the

Scheme 1. Mn(I)-Based Carbonyl Bipyridyl Molecular Catalysts Used in This Study

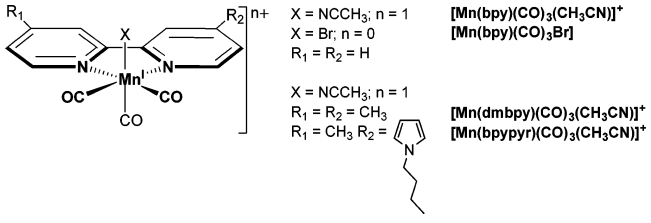

general voltammetric features related to the electrocatalytic process and the analysis of the stability of the different interfaces during controlled-potential preparative-scale electrolysis. Key parameters characterizing the physical properties of the different semiconductor/liquid junctions, such as the built-in voltage, the barrier height, or the depletion width within the space-charge layer, have been determined. Moreover, the energy conversion characteristics of each investigated system (fill factor and energy conversion efficiency) have also been quantified. Herein, we demonstrate that SiNWs−H stands as an efficient photocathode to perform the CO_2 electroreduction with respect to planar Si−H, showing better stability, double built-in voltages, and space-charge layer widths under electrocatalytic conditions, as well as higher fill factors and better energy conversion efficiencies.

Finally, as an ongoing work, we also present preliminary results on Mn-based modified SiNWs photocathodes prepared by electropolymerization of a new Mn molecular complex incorporating an N-functionalized pyrrole derivative (Scheme 1). Indeed, it is worth emphasizing that the transfer of the catalyst from the solution phase to solid interfaces is an essential prerequisite for technologically viable future applications related to electrocatalysis at photocathodes.

2. RESULTS AND DISCUSSION

2.1. Cyclic Voltammetry Studies. Electrochemical measurements were performed in CH_3CN + 0.1 M Bu_4NClO_4 under different conditions: argon, CO_2, and CO_2 + 5% v/v H_2O at Si−H and SiNWs−H photocathodes. Same experiments were also carried out at a glassy carbon electrode (GCE) considered as reference. Typical cyclic voltammograms (CVs) corresponding to the reduction of the Mn(I) tris-carbonyl complex [Mn(bpy) $(CO)_3(CH_3CN)](PF_6)$ (bpy = 2,2′-bipyridine) at flat Si−H and SiNWs−H in the dark and under irradiation through a red filter (λ > 600 nm; fluence: 20 mW cm^{-2}) are shown in Figure 1. The CVs obtained with the two other investigated Mn-based complexes, [Mn(bpy) $(CO)_3Br$] and [Mn(dmbpy) $(CO)_3(CH_3CN)](PF_6)$ (dmbpy = 4,4′-dimethyl-2,2′-bipyridine) are given in Figures S2 and S3 (Supporting Information).

The electrochemical behavior of these Mn(I) tricarbonyl complexes at GCE has already been reported by us.[17,34] Briefly,

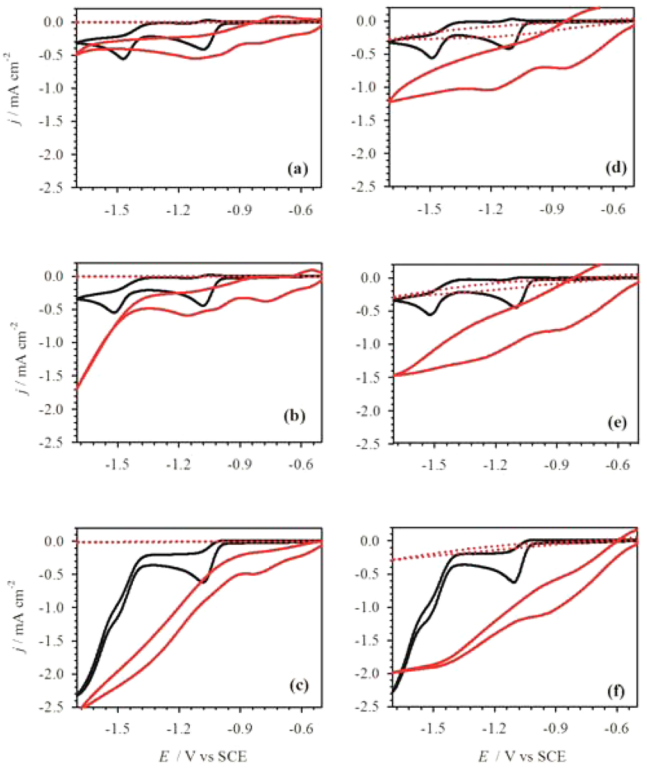

Figure 1. CVs of a solution of [Mn(bpy) $(CO)_3(CH_3CN)](PF_6)$ at 1 mM in CH_3CN + 0.1 M Bu_4NClO_4 at flat Si−H (left side panel) and SiNWs−H (right side panel) in the dark (dotted red lines) and under illumination through a red filter (20 mW cm^{-2}; solid red lines) under Ar (a, d), CO_2 (b, e) and CO_2 + 5% v/v H_2O (c, f). Black lines correspond to the CVs obtained at GCE. Potential scan rate: 0.1 V s^{-1}.

DOI: 10.1021/acscatal.5b01546
ACS Catal. 2015, 5, 6138−6147

in the cathodic potential range, they undergo two successive irreversible one-electron reduction waves (Figure 1a,b; black lines), leading to the formation of a dimer $[Mn^0(L)(CO_3)]_2$ (L: ligand) and the anionic mononuclear species $[Mn(L)(CO_3)]^-$, respectively, following eqs 1−3.

$$[Mn(L)(CO)_3(CH_3CN)]^+ + e^- \rightarrow [Mn(L)(CO)_3(CH_3CN)] \quad (1)$$

$$[Mn(L)(CO)_3CH_3CN)] \rightarrow 1/2[Mn(L)(CO)_3]_2 + CH_3CN \quad (2)$$

$$[Mn(L)(CO)_3]_2 + 2e^- \rightarrow 2[Mn(L)(CO)_3]^- \quad (3)$$

The addition of water to the CO_2-saturated electrolyte solution of $[Mn(bpy)(CO)_3(CH_3CN)](PF_6)$ causes an enhancement in the cathodic current (Figure 1c), which indicates the involvement of the reduced Mn dimer in the electrocatalytic process.[17]

A similar electrochemical behavior was observed at illuminated flat Si−H and SiNWs−H (Figure 1). The redox processes ascribed to the Mn complex are observed at less-negative potentials on SiNWs−H. We also notice the presence of a shoulder between the two principal cathodic peaks, which was observed only at flat Si−H (Figure 1a,b). The origin of this feature is thought to be due to a redox-active species like $[Mn(bpy)(CO)_3X]$ wherein an acetonitrile ligand would have been exchanged by a better electron-donating ligand, such as water, halogen, or also hydride, which could be present on the Si−H surface at the photoelectrode interface. This hypothesis seems reasonable because such features were not observed on the CVs of the Mn complex at either GCE or SiNWs−H electrode which were subjected to different surface treatment than flat Si−H.

The cathodic photocurrent density was slightly increased under CO_2 and more strongly increased under CO_2 in the presence of water. It must be underlined that the CVs at flat Si−H and SiNWs−H under CO_2 + 5% v/v H_2O are approximately S-shaped, more in the case of SiNWs−H for which this is a commonly encountered feature.[39] This reflects diffusion control (no kinetic constraints due to the catalytic reaction) by the mass transport of electroactive species to the silicon surface. In the case of SiNWs−H, it is highly likely that diffusion control within the nanowires network is more important leading to an accentuated S-shaped response. Moreover, the slower increase of the catalytic current at the semiconductor/electrolyte interface compared to GCE, as well as the distortion of the CVs observed for the semiconducting electrodes may be ascribed to some kinetic constraints for the charge transfer from the semiconductor to the catalyst. The cathodic peak potentials corresponding to the two redox systems of the studied Mn complexes at illuminated flat Si−H and SiNWs−H are gathered in Table 1 for the three media, together with those obtained at GCE.

From Figures 1, S2, and S3, it can be concluded that the cathodic photocurrent density values obtained at SiNWs−H are overall higher than those obtained at flat Si−H within the range −0.5 to −1.4 V vs SCE. For example, the photocurrent densities measured at −1.0 V vs SCE for $[Mn(bpy)(CO)_3(CH_3CN)](PF_6)$ reduced at illuminated flat Si−H and SiNWs−H are, respectively, 0.48 and 0.75 mA cm^{-2} under argon, 0.5 and 0.83 mA cm^{-2} under CO_2, and 0.7 and 1.14 mA cm^{-2} under CO_2 + 5% v/v H_2O. Such a trend can be attributed not only to the higher electrochemically active surface area of SiNWs−H compared with flat Si−H but also to their greater efficiency to decouple minority carrier generation and collection.[40] It is worth noting that the cathodic current corresponding to the reduction of the Mn complex at GCE is nearly zero at this potential (−1.0 V) in all media. These results actually support an activation of the electrocatalytic process by photogenerated minority charge carriers (namely, electrons) at illuminated silicon electrodes.

Table 1. Redox Peak Potentials for the Different Mn Carbonyl Complexes at 1 mM in CH_3CN + 0.1 M Bu_4NClO_4 (Figures 1, S2, and S3)[a]

$[Mn(bpy)(CO)_3(CH_3CN)](PF_6)$						
	GCE		Si−H		SiNWs−H	
medium	$E_{red,1}$	$E_{red,2}$	$E_{red,1}$	$E_{red,2}$	$E_{red,1}$	$E_{red,2}$
Ar	−1.07	−1.47	−0.82	−1.12	−0.85	−1.21
CO_2	−1.07	−1.50	−0.77	−1.16	−0.86	−1.23
CO_2 + 5% H_2O	−1.10	–	−0.83	–	−0.95	–
$[Mn(dmbpy)(CO)_3(CH_3CN)](PF_6)$						
	GCE		Si−H		SiNWs−H	
medium	$E_{red,1}$	$E_{red,2}$	$E_{red,1}$	E_{red2}	$E_{red,1}$	$E_{red,2}$
Ar	−1.21	−1.62	−0.90	−1.21	−0.95	−1.4
CO_2	−1.20	−1.64	−0.88	−1.16	–	–
CO_2 + 5% H_2O	–	–	–	–	–	–
$[Mn(bpy)(CO)_3Br]$						
	GCE		Si−H		SiNWs−H	
medium	$E_{red,1}$	$E_{red,2}$	$E_{red,1}$	E_{red2}	$E_{red,1}$	$E_{red,2}$
Ar	−1.23	−1.45	–	−1.22	−0.99	–
CO_2	−1.23	−1.45	–	−1.3	–	–
CO_2 + 5% H_2O	−1.22	–	–	–	–	–

[a]Values in V vs saturated calomel electrode (SCE). The semiconducting surfaces were irradiated through a red filter (20 mW cm^{-2}).

Similar features were observed for $[Mn(dmbpy)(CO)_3(CH_3CN)](PF_6)$ and $[Mn(bpy)(CO)_3Br]$ complexes, with higher photocurrent densities for the bpy analogue (Figure S2 and S3). UV−vis spectra of each Mn^I complex-containing electrolytic solution were performed before and after the analytical electrochemical measurements on illuminated SiNWs−H (Figure S4). The spectra showed the characteristic absorbance bands already reported for these complexes, including a shift in the absorbance band of $[Mn(bpy)(CO)_3Br]$ due to the formation of the corresponding Mn acetonitrile derivative by a solvolysis process eq 4.[17]

$$[Mn(L)(CO)_3Br] + CH_3CN \rightarrow [Mn(L)(CO)_3(CH_3CN)]^+ + Br^- \quad (4)$$

No degradation of the complexes over moderate irradiation periods (~90 min) was inferred from the spectra.

2.2. Energy Diagram of the Semiconductor/Electrolyte Interface at Equilibrium. To build the energy diagram of Si−H and SiNWs−H interfaces in equilibrium with the different molecular catalyst solutions, it is essential to estimate the flatband potential V_{fb} of the silicon surface, that is, the electrode potential for which there is no space-charge region in the semiconductor. Toward this goal, impedance spectroscopy measurements were performed in the dark under depletion conditions (i.e., depletion of valence band holes in the space charge region of the *p*-type surface). Under these conditions, V_{fb} can be estimated from the commonly used Mott−Schottky (MS) plot (C^{-2} vs E) that gives the space-charge capacitance C

DOI: 10.1021/acscatal.5b01546
ACS Catal. 2015, 5, 6138−6147

as a function of the electrode potential E (see Appendix in the SI).[41] From the intercept and the slope of a linear MS plot, the dopant density N_D and V_{fb} of a given semiconductor can be easily determined.

Figure 2 shows the different MS plots obtained for the molecular catalyst [Mn(dmbpy) $(CO)_3(CH_3CN)](PF_6)$ in the

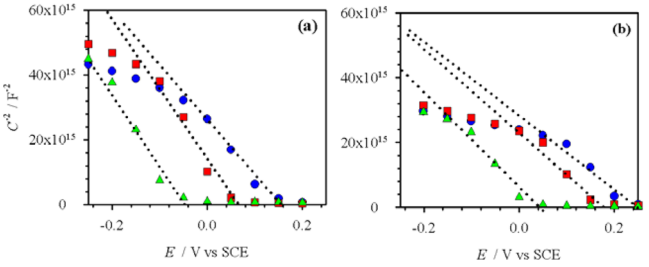

Figure 2. Mott−Schottky plots of flat Si−H (a) and SiNWs−H (b) in contact with a solution of [Mn(dmbpy) $(CO)_3(CH_3CN)](PF_6)$ at 1 mM in CH_3CN + 0.1 M Bu_4NClO_4, measured at a frequency of 50 kHz, under argon (blue circles), CO_2 (red squares) and CO_2 + 5% v/v H_2O (green triangles). Dotted lines represent the linear fittings. All measurements were performed in the dark.

three investigated media. For the sake of simplicity, only the MS plots measured at 50 kHz are shown, though several frequencies were applied giving comparable values of V_{fb} and N_D (SI).

Two slopes can be distinguished in the C^{-2} vs E plots, as already reported for other p-type silicon surfaces. These deviations from ideality are attributed to the critical dependence that p-type silicon exhibits on the initial surface treatment, in contrast to the case of n-type silicon.[42,43] The average V_{fb} values estimated from the first slope of the linear MS part at higher potentials, together with the open circuit potential values, OCP, measured in each medium are gathered in Table 2. V_{fb} was also estimated from the second slope of the MS plots, but the highly positive values obtained (>0.8 V vs SCE) were considered to be not relevant and therefore immediately discarded. An average value for the dopant density N_D of $(1.8 \pm 0.2) \times 10^{15}$ cm^{-3} was obtained from the first slope of the linear MS part, which matched adequately the resistivity value provided by the distributor.

Some trends can be drawn from such data. First, the V_{fb} values calculated for SiNWs−H in contact with [Mn(dmbpy) $(CO)_3(CH_3CN)](PF_6)$ are slightly more positive than those obtained with flat Si−H. This was not the case for the two other Mn-based complex homologues (Table 2) for which V_{fb} was found to not depend significantly on the structuring state of the silicon electrode. Second, a systematic decrease in both OCP and V_{fb} values when adding 5% of H_2O under CO_2 atmosphere was observed for all the tested systems with both silicon surfaces. For instance, the addition of water into a CO_2-saturated solution of [Mn(dmbpy) $(CO)_3(CH_3CN)](PF_6)$ led to a decrease in OCP of ca. 100 and 260 mV on Si−H and SiNWs−H, respectively, whereas the V_{fb} values decreased around 200 mV for both silicon electrodes. The first phenomenon (decrease in OCP) clearly indicates a change in the potential of the redox couple of the catalyst at equilibrium with the silicon surface, consistent with the involvement of a different intermediate between the Mn complex and CO_2 in the presence or absence of water.[34] The second phenomenon (decrease in V_{fb}) might be attributed to a partial oxidation of the silicon surface upon water addition, with the consequent

Table 2. Flatband Potentials V_{fb} and Open Circuit Potentials OCP (V vs SCE) Obtained from Solutions of the Different Mn Carbonyl Complexes at 1 mM in CH_3CN + 0.1 M Bu_4NClO_4[a]

[Mn(bpy) $(CO)_3(CH_3CN)](PF_6)$				
	Si−H		SiNWs−H	
medium	OCP/V	V_{fb}/V	OCP/V	V_{fb}/V
Ar	−0.28	0.10	−0.40	0.10
CO_2	−0.20	0.15	−0.38	0.08
CO_2 + 5% H_2O	−0.15	0.06	−0.52	−0.02
[Mn(dmbpy) $(CO)_3(CH_3CN)](PF_6)$				
	Si−H		SiNWs−H	
medium	OCP/V	V_{fb}/V	OCP/V	V_{fb}/V
Ar	−0.25	0.10	−0.35	0.20
CO_2	−0.24	0.02	−0.32	0.13
CO_2 + 5% H_2O	−0.36	−0.11	−0.49	−0.01
[Mn(bpy) $(CO)_3Br$]				
	Si−H		SiNWs−H	
medium	OCP/V	V_{fb}/V	OCP/V	V_{fb}/V
Ar	−0.29	0.07	−0.32	0.08
CO_2	−0.29	0.06	−0.31	0.07
CO_2 + 5% H_2O	−0.46	−0.08	−0.62	−0.07

[a]The V_{fb} values correspond to the average values determined from Mott-Schottky plots at three different frequencies: 50, 40, and 30 kHz. Relative uncertainty: ± 0.02 V.

generation of surface states leading to the nonideal situation of Fermi Level pinning.[44] All the OCP values obtained at SiNWs−H were systematically more negative than those obtained at Si−H, which implies the creation of a higher built-in voltage at the interface SiNWs/catalyst solution (Figure 3 and Table S1) and is in agreement with the higher cathodic photocurrent density values observed for SiNWs−H (Figure 1, S2 and S3). From the OCP, N_D and V_{fb} values gathered in Table 2, the different interfacial energetic parameters which characterize the semiconductor/solution system at electrochemical equilibrium can be calculated and be used to depict the corresponding energetic diagram (see Appendix for any detail). As an example, Figure 3 shows the energy diagram at the interface formed between a solution of [Mn(bpy) $(CO)_3Br$] and Si−H or SiNWs−H under argon, CO_2 and CO_2 + 5% v/v H_2O.

From these diagrams, it can be established that when Si−H or SiNWs−H are in equilibrium with the electrolytic solution, a downward band bending occurs, because the initial Fermi level of the isolated silicon (given by the V_{fb} value) is more positive than the equilibrium potential of the Mn^I/Mn^0 couple (given by the OCP value). The greater the difference between the initial electrochemical potentials of the semiconductor and solution phases is, the stronger will be the electric field generated at the space-charge layer of the semiconductor upon equilibration, and the longer will be its extension within the semiconductor bulk. Semiconductor/liquid junctions giving rise to high band bending degrees within the semiconductor are more efficient in decoupling minority carriers generation and collection (if inversion conditions are not reached)[45] and hence desirable for photoelectrocatalytic purposes. The degree of band bending within the semiconductor upon equilibration and the extension of the electric field can be quantified, respectively, by the built-in voltage V_{bi}, the barrier height ϕ_b, and the depletion width W(see SI). The values of V_{bi}, ϕ_b, and W

DOI: 10.1021/acscatal.5b01546
ACS Catal. 2015, 5, 6138−6147

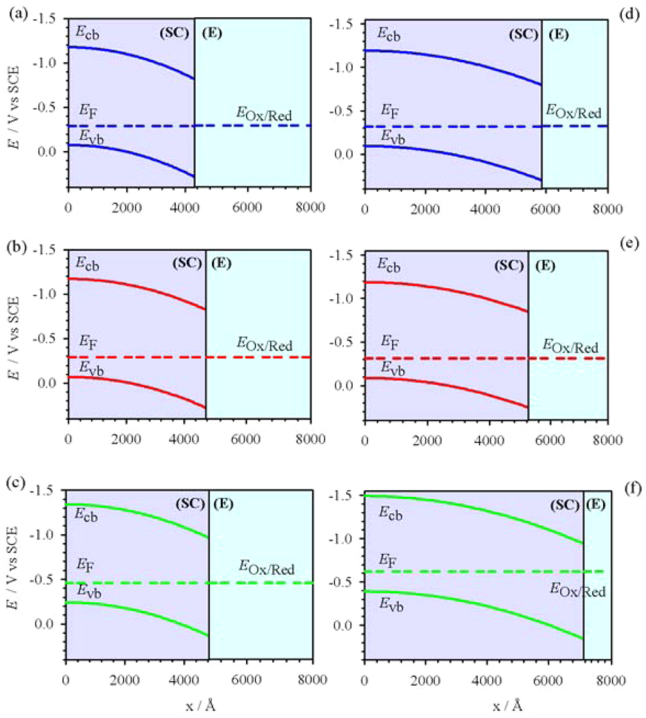

Figure 3. Energy diagrams at the interface formed between a solution of [Mn(bpy) $(CO)_3Br$] at 1 mM and Si−H (left side panel) or SiNWs−H (right side panel) under argon (a, d, blue lines), CO_2 (b, e, red lines) and CO_2 + 5% v/v H_2O (c, f, green lines). E_{cb}, E_{vb}, E_F, and $E_{Ox/Red}$ are defined in the Supporting Information (SI). SC: semiconductor, E: electrolytic solution.

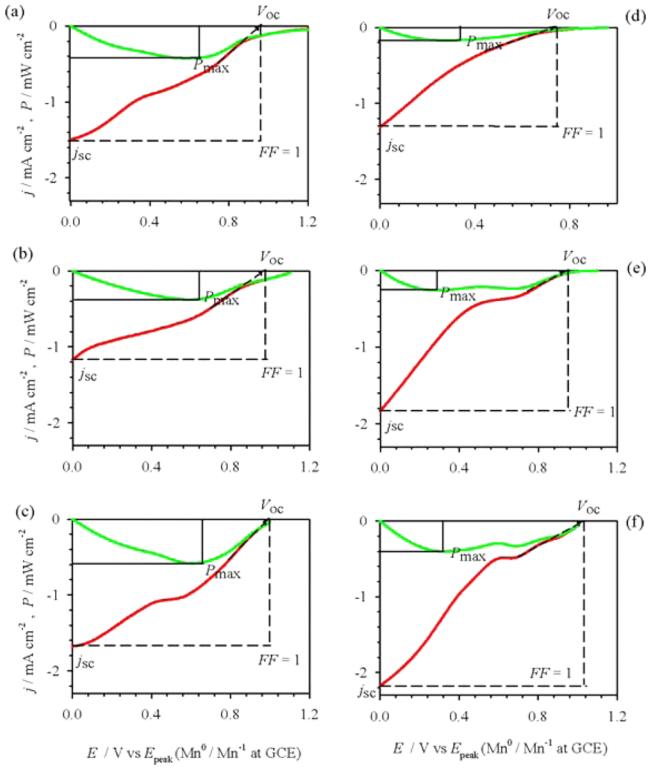

Figure 4. Photocurrent density−voltage (red lines) and power−voltage (green lines) plots corresponding to solutions of [Mn(bpy) $(CO)_3Br$] (a, d), [Mn(dmbpy) $(CO)_3(CH_3CN)](PF_6)$ (b, e) and [Mn(bpy) $(CO)_3(CH_3CN)](PF_6)$ (c, f) at 1 mM in CH_3CN + 0.1 M Bu_4NClO_4, under CO_2 + 5% v/v H_2O, at Si−H (left side panel) and SiNWs−H (right side panel). See SI for symbols and details. Note that the power is given by $P = |j \times V|$, though it has been plotted in the negative j axis for the sake of simplicity.

obtained for the three different molecular catalysts are gathered in Table S1 for both silicon electrodes. The knowledge of such parameters allows for a complete quantitative description of the energetics of each system under equilibrium conditions and is particularly useful to assess the suitability of the different systems for performing the photoelectrochemical reduction of CO_2. From the degree of band bending shown in Figure 3 and the values reported in Table S1, it is clear that the electric field inside the semiconductor is stronger for SiNWs−H compared with Si−H, even more in the presence of water, for which the space-charge region extends almost double inside the silicon bulk for SiNWs−H (compare Figure 3c and 3f). Moreover, by comparing the values of V_{bi}, ϕ_b, and W for both kinds of surfaces and following the reasoning given above, it can be concluded that under the condition selected for this study, SiNWs−H are always preferable to Si−H as photoelectrodes for the electroreduction of CO_2 in terms of efficiency in decoupling minority carriers generation and collection. On the other hand, for a given kind of surface, the V_{bi}, ϕ_b, and W values are similar for the three studied molecular catalysts (Table S1), which would indicate a comparable catalytic efficiency toward the CO_2 reduction.

2.3. Light to Electrical Energy Conversion Efficiency for CO_2 Photoelectroreduction. Figure 4 shows the photocurrent density−voltage and power−voltage plots obtained with the three molecular catalysts, under CO_2 + 5% v/v H_2O, at Si−H and SiNWs−H (left and right side panels, respectively). The values of the short-circuit photocurrent density j_{sc}, open-circuit potential under illumination V_{oc}, and maximum power drawn for the photoelectrochemical cell P_{max} for each system were calculated by following the procedure described in the SI.

The photocurrent density values required for building these plots were obtained by subtracting the first scan of the CVs recorded in the dark from that recorded under illumination for each system. Moreover, the potential of the second reduction peak of the Mn complexes at GCE was taken as the zero potential for the energy conversion calculations, because at this potential value, we can state that the light saturation regime (yielding the maximum photocurrent) has been reached within 5% error at the interface silicon/molecular catalyst solution, so it coincides with the potential of short-circuit photocurrent within this error. The fill factor FF and energy conversion efficiency η values calculated from these plots are gathered in Table 3.

Table 3. Fill Factor FF and Energy Conversion Efficiency η Values Obtained from the Photocurrent Density−Voltage Plots Given in Figure 4 for the Different Silicon/Molecular Catalyst Solution Interfaces under Electrocatalytic Conditions (CO_2 + 5% v/v H_2O)

	SiNWs−H		Si−H	
catalyst	FF	η/%	FF	η/%
[Mn(bpy) $(CO)_3Br$]	0.30	2.1	0.18	0.9
[Mn(dmbpy) $(CO)_3(CH_3CN)](PF_6)$	0.34	2.0	0.15	1.3
[Mn(bpy) $(CO)_3(CH_3CN)](PF_6)$	0.35	3.0	0.18	2.0

DOI: 10.1021/acscatal.5b01546
ACS Catal. 2015, 5, 6138−6147

The FF and η values obtained from these systems are in very good agreement with those reported for Ni or Pt nanoparticles coated *p*-type silicon photocathodes[46] or for *p*-type dye-sensitized solar cells.[47] As expected, the interface SiNWs−HI Mn complex solution exhibited higher FF and η with respect to Si−H, which is consistent with better electrocatalytic performances of this interface for the CO_2 reduction. Moreover, a greater catalytic efficiency of the complex [Mn(bpy) $(CO)_3(CH_3CN)](PF_6)$ can be noticed, as evidenced by a η higher than that calculated for the two other Mn complexes. Considering the difference between the energy of conduction band of silicon and the LUMO of the complex (ΔG) as the driving force for the rate of interfacial electron transfer,[48,49] the greater efficiency of [Mn(bpy) $(CO)_3CH_3CN](PF_6)$ is not surprising and can be ascribed to a lower value of the LUMO of this complex (−1.07 V for the first reduction process at GCE under argon, Table 1) compared with that of the two other complexes. Nevertheless, this is not the only criterion that contributes to the electrocatalytic efficiency, in fact, the electrocatalytic reduction of CO_2 using the dmbpy complexes could proceed through two distinct pathways depending on the catalysis potential, as previously demonstrated.[17]

2.4. Stability of the Silicon/Electrolyte Interface under Photoelectrocatalytic Conditions. In order to test the stability of the different silicon/electrolyte interfaces, chronoamperometric experiments in which the light source was successively switched ON/OFF during periods of 60 and 120 s, respectively, were performed at different reduction potentials, under CO_2 + 5% v/v H_2O with vigorous stirring. Figure 5 shows the chronoamperometric curves obtained under ON/OFF (120 s/60 s) illumination cycles for the complex [Mn(bpy) $(CO)_3Br$] at Si−H and SiNWs−H, together with the corresponding chronocoulometric responses.

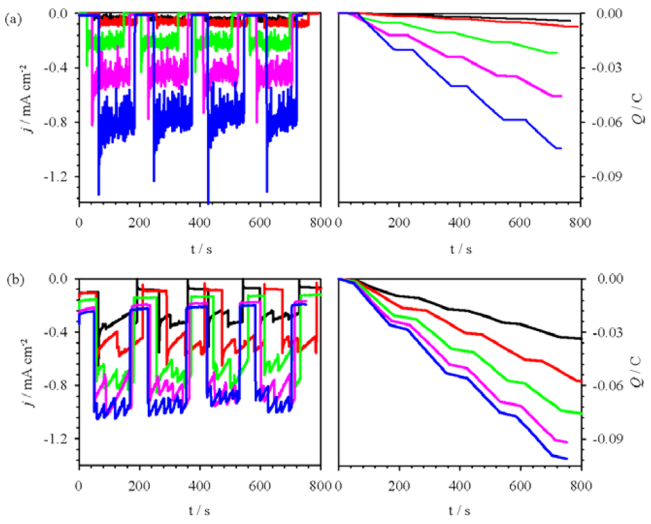

Figure 5. Chronoamperometric (*j*−*t*, left side panel) and chronocoulometric (*Q*−*t*, right side panel) curves corresponding to the electroreduction of [Mn(bpy) $(CO)_3Br$] at flat Si−H (a) or SiNWs−H (b) during several ON/OFF light switching cycles. Applied voltage: −0.7 (black lines), −0.8 (red lines), −1.0 (green lines), −1.2 (pink lines), and −1.4 (blue lines) V vs SCE. Conditions: 1 mM of complex in CH_3CN + 0.1 M Bu_4NClO_4 under CO_2 + 5% v/v H_2O. The noise in the chronoamperometric signals can be ascribed to the removing of small produced gas bubbles from the Si−H and SiNWs−H electrodes.

The photocurrent densities measured at SiNWs−H were higher and more stable than those measured at Si−H. It must be noticed that at moderately cathodic potentials (until −1.0 V vs SCE), for which small or no photocurrent was observed at Si−H, appreciable photocurrent values could be measured on SiNWs−H. Similar behavior was observed with [Mn(bpy) $(CO)_3(CH_3CN)](PF_6)$ and [Mn(dmbpy) $(CO)_3(CH_3CN)](PF_6)$, with photocurrent density values slightly higher for the dmbpy analogue. Therefore, on the basis of these observations and electrochemical data (vide supra), we can state that SiNWs−H is a more efficient photocathode than Si−H for the CO_2 electrocatalytic reduction with Mn-carbonyl molecular catalysts in solution.

2.5. Preparative Scale Electrolysis. To obtain further insights on the catalytic activity of the investigated Mn-based complexes, preparative-scale electrolysis was carried out by using the most efficient photocathode, namely SiNWs−H, as the working electrode. Thus, controlled-potential electrolysis experiments were carried out at −1.10 V vs SCE with [Mn(bpy) $(CO)_3Br$] or [Mn(dmbpy) $(CO)_3(CH_3CN)](PF_6)$ at 1 mM in CH_3CN + 0.1 M Bu_4NClO_4 under CO_2 + 5% v/v H_2O in a tightly closed electrochemical cell. The gas composition inside the cell was analyzed at regular time intervals by gas chromatography (GC) to follow the selectivity of the electrocatalytic process. Additionally, analysis of the electrolyte solution by HPLC was carried out at the end of the electrolysis to determine the possible presence of formate.

Both bpy and dmbpy derivatives led to quantitative faradaic efficiency toward the selective production of CO without generation of H_2 or formate. The measured photocurrents remained stable during the electrolysis time (3 h for the bpy analogue and 5 h for the dmbpy derivative). Nevertheless, the UV−vis spectra of the Mn complexes before and after electrolysis evidenced partial degradation of the catalysts, possibly caused by a long exposition to light, particularly for the bpy derivative. For this catalyst, approximately half of the catalyst was lost after 3 h electrolysis, whereas no significant degradation was observed after 5 h electrolysis for the dmbpy analogue. The turnover frequency (TOF) corresponding to these two systems was calculated following two expressions to take into account both the role of the semiconductor as photocatalyst as well as that of the molecular electrocatalyst in solution. The first expression uses the formalism available for heterogeneous catalysts, as previously reported for the CO_2 catalytic reduction at a silicon surface[33,50,51] (see SI for more information). The corresponding TOF numbers are given in Figure 6 as a function of the electrolysis time.

The TOF, available for homogeneous catalysts, was based on the amount of produced CO during the electrolysis experiment. In this context, the amount of generated CO (determined by GC) was found to be 0.663 and 0.415 mol × mol^{-1} of catalyst × h^{-1} for the bpy and dmbpy analogues, respectively. The lack of expressions characterizing the surface concentrations of the electroactive catalytic species at the semiconductor/liquid junction impedes a more accurate calculation of the TOF, as proposed by Costentin et al.[15,52] It must be underlined here that, up to date, there is no expression for the TOF number taking into account together the contributions of both semiconductor and molecular electrocatalyst.

Therefore, from the analytical and preparative electrochemical studies, it can be concluded that the bpy analogues are molecular catalysts more efficient than the dmbpy one to perform the electroreduction of CO_2 at −1.10 V at illuminated

DOI: 10.1021/acscatal.5b01546
ACS Catal. 2015, 5, 6138−6147

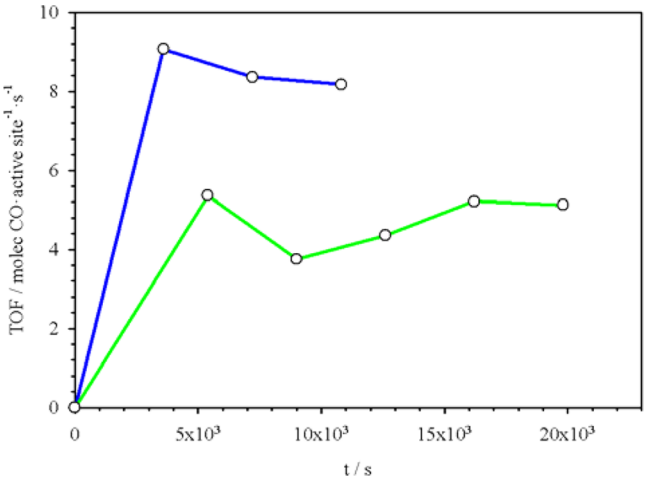

Figure 6. TOF–time plots for the bulk electrolysis of [Mn(bpy)$(CO)_3$Br] (blue line) or [Mn(dmbpy)$(CO)_3(CH_3CN)](PF_6)$ (green line) at 1 mM in CH_3CN + 0.1 M Bu_4NClO_4 under CO_2 + 5% v/v H_2O, calculated by using the heterogeneous photocatalyst definition (see SI for details).

Si–H or SiNWs–H. The controlled-potential electrolysis experiments evidenced however a higher robustness of the dmbpy derivative during several hours of photoelectrocatalysis.

2.6. Electrocatalytic Reduction of CO_2 at Catalyst-Modified SiNWs–H Photoelectrodes. Finally, to take a considerable step toward the design of catalytic interfaces incorporating Mn-based bipyridyl carbonyl complexes for the CO_2 reduction, we report here an original modification route combining a nanostructured SiNWs–H electrode and a Mn-carbonyl based complex. This hybrid photocathode consisting of *N*-functionalized polypyrrole (ppyr) film deposited onto SiNWs–H was prepared from the electropolymerization of a new pyrrole based Mn complex ([Mn(bpypyr)$(CO)_3(CH_3CN)](PF_6)$, Scheme 1; see SI for synthesis details) on SiNWs–H. Equivalent rebased pyr complexes, containing the same substituted bpy ligand, were synthesized by our group in the 80s to elaborate *N*-functionalized ppyr-modified Pt cathodes for electrocatalytic reduction of CO_2.[53,54]

Compared with the homogeneous catalysis, let us recall that a great practical interest of electrocatalysis at modified electrodes is that it does not require purification steps to retrieve the catalytic species. Thus, it gives the opportunity to work in different media, even those where the catalyst is not soluble, like water for instance. There are only few reports concerning the electrochemical deposition of conductive polymers onto SiNWs, and most of them are related to the electropolymerization of thiophene derivatives for applications in lithium batteries and supercapacitors.[55,56]

The successive CVs obtained during the potentiodynamic electropolymerization of [Mn(bpypyr)$(CO)_3(CH_3CN)](PF_6)$ on SiNWs–H in CH_3CN + 0.1 M Bu_4NClO_4 are shown in Figure 7a. The SEM images corresponding to SiNWs–H before and after the polymer deposit are depicted in Figure 7b,c.

During the successive scans, the electrochemical oxidation of the pyr group led to the deposition of the corresponding redox-active Mn-substituted ppyr film onto SiNWs–H, as evidenced by the progressive growth of quasi-reversible redox processes in the range of 0.0–1.0 V (Figure 7a). The current densities associated with the two redox processes of the Mn center

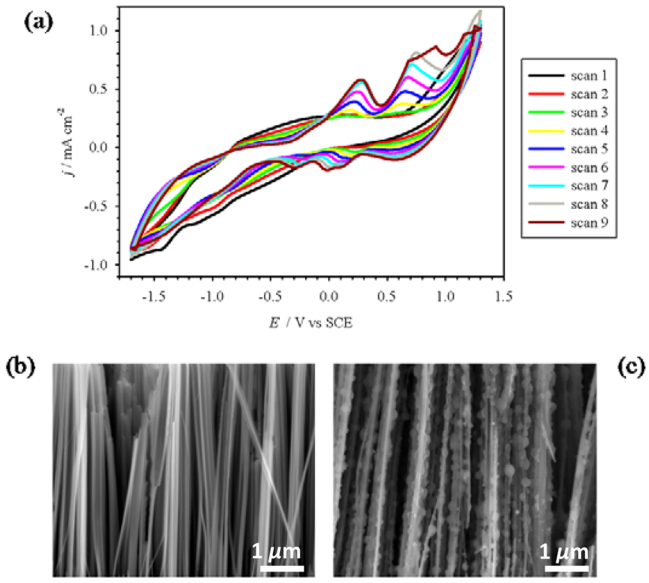

Figure 7. (a) CVs at 0.01 V s^{-1} corresponding to the potentiodynamic electropolymerization of [Mn(bpypyr)$(CO)_3(CH_3CN)](PF_6)$ at 1 mM in CH_3CN + 0.1 M Bu_4NClO_4 onto illuminated SiNWs–H. (b, c) SEM images of SiNWs–H before (b) and after the electropolymerization step (c).

(cathodic peaks around −1.4 and −1.0 V) decreased slightly in the course of electropolymerization during the four first scans and then became stable. The SEM images of Mn catalyst-modified SiNWs–H showed a granular morphology for the polymer (Figure 7c), covering homogeneously the vertical sidewalls of SiNWs. This type of homogeneous globular deposit is in agreement with the morphology observed for a nonfunctionalized ppyr coating onto silicon nanotrees and recently reported by Aradilla et al.[57] The electrochemical properties of the SiNWs–H photoelectrode modified by the Mn-ppyr functionalized film were analyzed in a monomer-free electrolytic solution (Figure 8a). In the anodic range, a stable quasi-reversible redox system at ca. 0.6 V was observed. It corresponds to the reversible oxidation of the ppyr matrix (doping/undoping process) of the electrogenerated film. This provides further evidence for the presence of a durably attached electroactive deposit.

In the cathodic range, the voltammetric responses of the two successive redox systems of immobilized Mn^I species were maintained under argon, as observed for the similar complex in solution (Figure 1a,d, Figure S2a,d and Figure S3a,d). Upon the addition of CO_2 and then H_2O, an enhancement in the cathodic photocurrent density was observed, in agreement with a catalytic activity of the modified photoelectrode. These preliminary results are promising and demonstrate the validity of the electropolymerization approach to elaborate hybrid molecular SiNWs–H-modified photocathodes for catalytic applications. We are now pursuing this research by studying in detail the electropolymerization process in view of developing Mn complex-functionalized ppyr-modified Si–H and SiNWs–H cathodes, as effective as possible, for photo-assisted electrocatalytic reduction of CO_2.

3. CONCLUSIONS

The electrochemical reduction of CO_2 at illuminated flat Si–H and SiNWs–H photocathodes has been investigated in CH_3CN medium by cyclic voltammetry, in the presence of three Mn-

DOI: 10.1021/acscatal.5b01546
ACS Catal. 2015, 5, 6138–6147

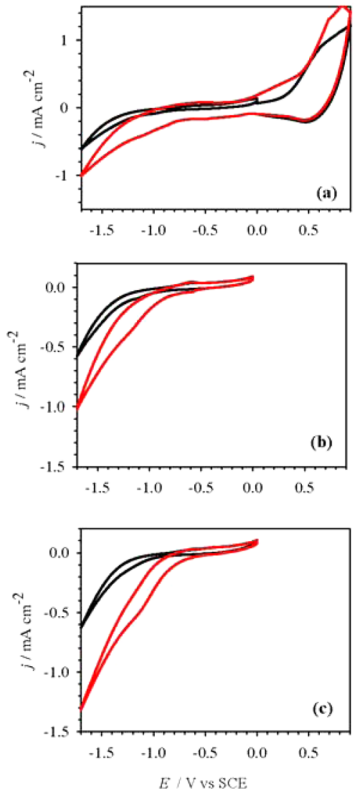

Figure 8. CVs of the electrocatalytic Mn-based polymeric film deposited onto SiNWs−H in CH_3CN + 0.1 M Bu_4NClO_4, in the dark (black lines) and under illumination through a red filter (red lines) and under argon (a), CO_2 (b), and CO_2 + 5% v/v H_2O (c). Potential scan rate: 0.02 V s^{-1}.

based carbonyl bipyridyl molecular complexes acting as homogeneous catalysts. The electrochemical data have clearly demonstrated the higher efficiency of the semiconducting photoelectrodes versus conventional working electrodes (e.g., GCE) in terms of energy consumption. From the energetic diagrams of the different semiconductor|liquid junctions, it can be concluded that the degree of band bending and the depth of the space-charge layer is always greater for SiNWs−H than for flat Si−H, being double under electrocatalytic conditions (CO_2 + 5% v/v H_2O). Interestingly, the efficiency of the light to electrical energy conversion and fill factor calculated under catalytic conditions have been higher for the nanostructured surface, owing to the higher electrochemically active surface area of SiNWs and its higher capacity to decouple minority carrier generation and collection. Bulk electrolysis at controlled potential has shown the quantitative conversion of CO_2 to CO, with no significant and 50% light-induced degradation for the dmbpy and bpy derivatives, respectively, at the end of photoassisted electrolysis. Finally, the electropolymerization of a new Mn-based pyrrole monomer onto the SiNWs−H photocathode has been successfully performed. The film has been found to be homogeneously electrodeposited along the wires of SiNWs and has retained the electrochemical activity of the Mn complex in hydro-organic solution under Ar and in the presence of CO_2. Work is currently in progress in order to study the selectivity of the electrocatalytic reduction of CO_2 with these novel modified photoelectrodes.

■ ASSOCIATED CONTENT

Supporting Information

The Supporting Information is available free of charge on the ACS Publications website at DOI: 10.1021/acscatal.5b01546.

Experimental procedures, synthesis of the electropolymerizable Mn-based pyrrole derivative, preparation of Si-NWs, selection of the irradiation wavelength for the electrocatalytic reduction of CO_2 at Si-NWs, appendix for the determination of the energy diagrams, light to electrical energy conversion efficiency and TOF number, CVs of $[Mn(bpy)(CO)_3]Br$ and $[Mn(dmbpy)(CO)_3(CH_3CN)](PF_6)$ at flat Si−H and Si-NWs-H (PDF)

■ AUTHOR INFORMATION

Corresponding Authors

*E-mail: sylvie.chardon@ujf-grenoble.fr.
*E-mail: bruno.fabre@univ-rennes1.fr.

Notes

The authors declare no competing financial interest.

■ ACKNOWLEDGMENTS

E.T.-P. thanks the University of Rennes 1 for financial support ("Stratégie et Attractivité Durable" SAD 2013 and "Projets Scientifiques Emergents" 2015). G. Li is acknowledged for his help in the preparation of Si-NWs. The authors are also grateful to the assistance of F. Gouttefangeas for SEM images performed at CMEBA (ScanMAT, University of Rennes 1, France) which received a financial support from the Région Bretagne and European Union (CPER-FEDER 2007-2014). The authors acknowledge support from ICMG FR 2607 and LabEx ARCANE (ANR-11-LABX-0003-01). The authors gratefully acknowledge Dr. C.E. Castillo and Dr. M. Bourrez for their contribution to the earliest experiments on the Mn-substituted pyrrole derivative.

■ REFERENCES

(1) Aresta, M.; Dibenedetto, A.; Angelini, A. Catalysis for the Valorization of Exhaust Carbon: from CO_2 to Chemicals, Materials, and Fuels. Technological Use of CO_2. *Chem. Rev.* **2014**, *114*, 1709−1742.

(2) Appel, A. M.; Bercaw, J. E.; Bocarsly, A. B.; Dobbek, H.; DuBois, D. L.; Dupuis, M.; Ferry, J. G.; Fujita, E.; Hille, R.; Kenis, P. J. A.; Kerfeld, C. A.; Morris, R. H.; Peden, C. H. F.; Portis, A. R.; Ragsdale, S. W.; Rauchfuss, T. B.; Reek, J. N. H.; Seefeldt, L. C.; Thauer, R. K.; Waldrop, G. L. Frontiers, Opportunities, and Challenges in Biochemical and Chemical Catalysis of CO_2 Fixation. *Chem. Rev.* **2013**, *113*, 6621−6658.

(3) Styrring, P.; Jansen, D. *Carbon Capture and Utilisation in the Green Economy*; The Centre for Low Carbon Futures: The Netherlands, 2011; ISBN: 978-0-9572588-1-5.

(4) Aresta, M. *Carbon Dioxide as a Chemical Feedstock*; Wiley-VCH: Weinheim, 2010.

(5) Omae, I. Recent Developments in Carbon Dioxide Utilization for the Production of Organic Chemicals. *Coord. Chem. Rev.* **2012**, *256*, 1384−1405.

(6) Olajire, A. A. Valorization of Greenhouse Carbon Dioxide Emissions into Value-Added Products by Catalytic Processes. *J. CO2 Utilization* **2013**, *3*−*4*, 74−92.

(7) Ampelli, C.; Perathoner, S.; Centi, G. CO_2 Utilization: an Enabling Element to Move to a Resource- and Energy-Efficient Chemical and Fuel Production. *Philos. Trans. R. Soc., A* **2015**, *373*, 20140177.

DOI: 10.1021/acscatal.5b01546
ACS Catal. 2015, 5, 6138−6147

(8) Kumar, B.; Llorente, M.; Froehlich, J.; Dang, T.; Sathrum, A.; Kubiak, C. P. Photochemical and Photoelectrochemical Reduction of CO_2. *Annu. Rev. Phys. Chem.* **2012**, *63*, 541−569.
(9) Highfield, J. Advances and Recent Trends in Heterogeneous Photo(Electro)-Catalysis for Solar Fuels and Chemicals. *Molecules* **2015**, *20*, 6739−6793.
(10) Windle, C. D.; Perutz, R. N. Advances in Molecular Photocatalytic and Electrocatalytic CO_2 Reduction. *Coord. Chem. Rev.* **2012**, *256*, 2562−2570.
(11) Izumi, Y. Recent Advances in the Photocatalytic Conversion of Carbon Dioxide to Fuels with Water and/or Hydrogen using Solar Energy and Beyond. *Coord. Chem. Rev.* **2013**, *257*, 171−186.
(12) Qiao, J.; Liu, Y.; Hong, F.; Zhang, J. A Review of Catalysts for the Electroreduction of Carbon Dioxide to Produce Low-Carbon Fuels. *Chem. Soc. Rev.* **2014**, *43*, 631−675.
(13) Finn, C.; Schnittger, S.; Yellowlees, L. J.; Love, J. B. Molecular Approaches to the Electrochemical Reduction of Carbon Dioxide. *Chem. Commun.* **2012**, *48*, 1392−1399.
(14) Fenwick, A. Q.; Gregoire, J. M.; Luca, O. R. Electrocatalytic Reduction of Nitrogen and Carbon Dioxide to Chemical Fuels: Challenges and Opportunities for a Solar Fuel Device. *J. Photochem. Photobiol., B* **2015**, DOI: 10.1016/j.jphotobiol.2014.12.019.
(15) Costentin, C.; Robert, M.; Saveant, J. M. Catalysis of the Electrochemical Reduction of Carbon Dioxide. *Chem. Soc. Rev.* **2013**, *42*, 2423−2436.
(16) Costentin, C.; Passard, G.; Robert, M.; Saveant, J. M. Ultraefficient Homogeneous Catalyst for the CO_2-to-CO Electrochemical Conversion. *Proc. Natl. Acad. Sci. U. S. A.* **2014**, *111*, 14990−14994.
(17) Bourrez, M.; Molton, F.; Chardon-Noblat, S.; Deronzier, A. [Mn(bipyridyl) $(CO)_3Br$]: an Abundant Metal Carbonyl Complex as Efficient Electrocatalyst for CO_2 Reduction. *Angew. Chem., Int. Ed.* **2011**, *50*, 9903−9906.
(18) Sieh, D.; Lacy, D. C.; Peters, J. C.; Kubiak, C. P. Reduction of CO_2 by Pyridine Monoimine Molybdenum Carbonyl Complexes: Cooperative Metal-Ligand Binding of CO_2. *Chem. - Eur. J.* **2015**, *21*, 8497−8503.
(19) Kang, P.; Zhang, S.; Meyer, T. J.; Brookhart, M. Rapid Selective Electrocatalytic Reduction of Carbon Dioxide to Formate by an Iridium Pincer Catalyst Immobilized on Carbon Nanotube Electrodes. *Angew. Chem.* **2014**, *126*, 8853−8857.
(20) Whipple, D. T.; Kenis, P. J. A. Prospects of CO_2 Utilization via Direct Heterogeneous Electrochemical Reduction. *J. Phys. Chem. Lett.* **2010**, *1*, 3451−3458.
(21) Inglis, J. L.; MacLean, B. J.; Pryce, M. T.; Vos, J. G. Electrocatalytic Pathways Towards Sustainable Fuel Production from Water and CO_2. *Coord. Chem. Rev.* **2012**, *256*, 2571−2600.
(22) Schneider, J.; Jia, H.; Kobiro, K.; Cabelli, D. E.; Muckerman, J. T.; Fujita, E. Nickel(II) Macrocycles: Highly Efficient Electrocatalysts for the Selective Reduction of CO_2 to CO. *Energy Environ. Sci.* **2012**, *5*, 9502−9510.
(23) Thoi, V. S.; Chang, C. J. Nickel *N*-Heterocyclic Carbene−Pyridine Complexes that Exhibit Selectivity for Electrocatalytic Reduction of Carbon Dioxide over Water. *Chem. Commun.* **2011**, *47*, 6578−6580.
(24) Beley, M.; Collin, J. P.; Ruppert, R.; Sauvage, J.-P. Electrocatalytic Reduction of Carbon Dioxide by Nickel Cyclam^{2+} in Water: Study of the Factors Affecting the Efficiency and the Selectivity of the Process. *J. Am. Chem. Soc.* **1986**, *108*, 7461−7467.
(25) Hawecker, J.; Lehn, J.-M.; Ziessel, R. Electrocatalytic Reduction of Carbon Dioxide Mediated by Re(bipy) $(CO)_3Cl$ (bipy = 2,2′-bipyridine). *J. Chem. Soc., Chem. Commun.* **1984**, 328−330.
(26) Kumar, B.; Smieja, J. M.; Kubiak, C. P. Photoreduction of CO_2 on p-Type Silicon Using Re(bipy-But) $(CO)_3Cl$: Photovoltages Exceeding 600 mV for the Selective Reduction of CO_2 to CO. *J. Phys. Chem. C* **2010**, *114*, 14220−14223.
(27) Kumar, B.; Smieja, J. M.; Sasayama, A. F.; Kubiak, C. P. Tunable, Light-Assisted Co-Generation of CO and H_2 from CO_2 and H_2O by Re(bipy-tbu) $(CO)_3Cl$ and *p*-Si in Non-Aqueous Medium. *Chem. Commun.* **2012**, *48*, 272−274.
(28) Arai, T.; Sato, S.; Uemura, K.; Morikawa, T.; Kajino, T.; Motohiro, T. Photoelectrochemical Reduction of CO_2 in Water Under Visible-Light Irradiation by a p-Type InP Photocathode Modified with an Electropolymerized Ruthenium Complex. *Chem. Commun.* **2010**, *46*, 6944−6946.
(29) Sato, S.; Arai, T.; Morikawa, T.; Uemura, K.; Suzuki, T. M.; Tanaka, H.; Kajino, T. Selective CO_2 Conversion to Formate Conjugated with H_2O Oxidation Utilizing Semiconductor/Complex Hybrid Photocatalysts. *J. Am. Chem. Soc.* **2011**, *133*, 15240−15243.
(30) Sahara, G.; Abe, R.; Higashi, M.; Morikawa, T.; Maeda, K.; Ueda, Y.; Ishitani, O. Photoelectrochemical CO_2 Reduction using a Ru(II)−Re(I) Multinuclear Metal Complex on a p-Type Semiconducting NiO Electrode. *Chem. Commun.* **2015**, *51*, 10722−10725.
(31) Liu, R.; Stephani, C.; Han, J. J.; Tan, K. L.; Wang, D. Silicon Nanowires Show Improved Performance as Photocathode for Catalyzed Carbon Dioxide Photofixation. *Angew. Chem., Int. Ed.* **2013**, *52*, 4225−4228.
(32) Huang, Z.; Geyer, N.; Werner, P.; de Boor, J.; Gosele, U. Metal-Assisted Chemical Etching of Silicon: a Review. *Adv. Mater.* **2011**, *23*, 285−308.
(33) Liu, R.; Yuan, G.; Joe, C. L.; Lightburn, T. E.; Tan, K. L.; Wang, D. Silicon Nanowires as Photoelectrodes for Carbon Dioxide Fixation. *Angew. Chem., Int. Ed.* **2012**, *51*, 6709−6712.
(34) Bourrez, M.; Orio, M.; Molton, F.; Vezin, H.; Duboc, C.; Deronzier, A.; Chardon-Noblat, S. Pulse-EPR Evidence of a Manganese(II) Hydroxycarbonyl Intermediate in the Electrocatalytic Reduction of Carbon Dioxide by a Manganese Bipyridyl Derivative. *Angew. Chem., Int. Ed.* **2014**, *53*, 240−243.
(35) Walsh, J. J.; Neri, G.; Smith, C. L.; Cowan, A. J. Electrocatalytic CO_2 Reduction with a Membrane Supported Manganese Catalyst in Aqueous Solution. *Chem. Commun.* **2014**, *50*, 12698−12701.
(36) Agarwal, J.; Shaw, T. W.; Schaefer, H. F.; Bocarsly, A. B. Design of a Catalytic Active Site for Electrochemical CO_2 Reduction with Mn(I)-Tricarbonyl Species. *Inorg. Chem.* **2015**, *54*, 5285−5294.
(37) Lam, Y. C.; Nielsen, R. J.; Gray, H. B.; Goddard, W. A. A Mn Bipyrimidine Catalyst Predicted To Reduce CO_2 at Lower Overpotential. *ACS Catal.* **2015**, *5*, 2521−2528.
(38) Vollmer, M. V.; Machan, C. W.; Clark, M. L.; Antholine, W. E.; Agarwal, J.; Schaefer, H. F., III; Kubiak, C. P.; Walensky, J. R. Synthesis, Spectroscopy, and Electrochemistry of (α-Diimine)M-$(CO)_3Br$, M = Mn, Re, Complexes: Ligands Isoelectronic to Bipyridyl Show Differences in CO_2 Reduction. *Organometallics* **2015**, *34*, 3−12.
(39) Dai, P.; Xie, J.; Mayer, M. T.; Yang, X.; Zhan, J.; Wang, D. Solar Hydrogen Generation by Silicon Nanowires Modified with Platinum Nanoparticle Catalyst by Atomic Layer Deposition. *Angew. Chem., Int. Ed.* **2013**, *52*, 11119−11123.
(40) Oh, I.; Kye, J.; Hwang, S. Enhanced Photoelectrochemical Hydrogen Production from Silicon Nanowire Array Photocathode. *Nano Lett.* **2012**, *12*, 298−302.
(41) Zhang, X. G. *Electrochemistry of Silicon and its Oxide*; Kluwer Academic Publishers: New York, 2004.
(42) Aureau, D.; Moraillon, A.; Henry de Villeneuve, C.; Ozanam, F.; Allongue, P.; Chazalviel, J.-N.; Rappich, J. Electronic Properties and pH Stability of Si(111) Alkyl Monolayers. *ECS Trans.* **2009**, *19*, 373−379.
(43) Michalak, D. J.; Gstrein, F.; Lewis, N. S. Interfacial Energetics of Silicon in Contact with 11 M NH_4F(aq), Buffered HF(aq), 27 M HF (aq), and 18 M H_2SO_4. *J. Phys. Chem. C* **2007**, *111*, 16516−16532.
(44) Bard, A. J.; Bocarsly, A. B.; Fan, F. R. F.; Walton, E. G.; Wrighton, M. S. The Concept of Fermi Level Pinning at Semiconductor/Liquid Junctions. Consequences for Energy Conversion Efficiency and Selection of Useful Solution Redox Couples in Solar Devices. *J. Am. Chem. Soc.* **1980**, *102*, 3671−3677.
(45) *Encyclopedia of Electrochemistry: Semiconductor Electrodes and Photoelectrochemistry*; Bard, A. J., Stratmann, M., Licht, S., Eds.; Wiley-VCH: New York, 2002; Vol. 6.

DOI: 10.1021/acscatal.5b01546
ACS Catal. 2015, 5, 6138−6147

(46) Huang, Z.; McKone, J. R.; Xiang, C.; Grimm, R. L.; Warren, E. L.; Spurgeon, J. M.; Lewerenz, H. J.; Brunschwig, B. S.; Lewis, N. S. Comparison Between the Measured and Modeled Hydrogen-Evolution Activity of Ni- or Pt- Coated Silicon Photocathodes. *Int. J. Hydrogen Energy* **2014**, *39*, 16220−16226.
(47) Perera, I. R.; Daeneke, T.; Makuta, S.; Yu, Z.; Tachibana, Y.; Mishra, A.; Bäuerle, P.; Ohlin, A.; Bach, U.; Spiccia, L. Application of the Tris(Acetylacetonato)Iron(III)/(II) Redox Couple in p-Type Dye-Sensitized Solar Cell. *Angew. Chem., Int. Ed.* **2015**, *54*, 3758−3762.
(48) Huang, J.; Stockwell, D.; Huang, Z.; Mohler, D. L.; Lian, T. Photoinduced Ultrafast Electron Transfer from CdSe Quantum Dots to Re-bipyridyl Complexes. *J. Am. Chem. Soc.* **2008**, *130*, 5632−5633.
(49) Sato, S.; Morikawa, T.; Saeki, S.; Kajino, T.; Motohiro, T. Visible-Light-Induced Selective CO_2 Reduction Utilizing a Ruthenium Complex Electrocatalyst Linked to a p-Type Nitrogen-Doped Ta_2O_5 Semiconductor. *Angew. Chem., Int. Ed.* **2010**, *49*, 5101−5105.
(50) Habisreutinger, S. N.; Schmidt-Mende, L.; Stolarczyk, J. K. Photocatalytic Reduction of CO_2 on TiO_2 and other Semiconductors. *Angew. Chem., Int. Ed.* **2013**, *52*, 7372−7408.
(51) Serpone, N.; Salinaro, A.; Emeline, A.; Ryabchuk, V. Turnovers and Photocatalysis. A Mathematical Description. *J. Photochem. Photobiol., A* **2000**, *130*, 83−94.
(52) Costentin, C.; Passard, G.; Saveant, J. M. Benchmarking of Homogeneous Electrocatalysts: Overpotential, Turnover Frequency, Limiting Turnover Number. *J. Am. Chem. Soc.* **2015**, *137*, 5461−5467.
(53) Cosnier, S.; Deronzier, A.; Moutet, J.-C. Electrochemical Coating of a Platinum Electrode by a Poly(pyrrole) Film Containing the fac-Re(2,2′-bipyridine) $(CO)_3Cl$ System. Application to Electrocatalytic Reduction of CO_2. *J. Electroanal. Chem. Interfacial Electrochem.* **1986**, *207*, 315−321.
(54) Cosnier, S.; Deronzier, A.; Moutet, J.-C. Electrocatalytic Reduction of CO_2 on Electrodes Modified by fac-Re(2,2′-bipyridine) $(CO)_3Cl$ Complexes Bonded to Polypyrrole Films. *J. Mol. Catal.* **1988**, *45*, 381−391.
(55) Yao, Y.; Liu, N.; McDowell, M. T.; Pasta, M.; Cui, Y. Improving the Cycling Stability of Silicon Nanowire Anodes with Conducting Polymer Coatings. *Energy Environ. Sci.* **2012**, *5*, 7927−7930.
(56) Aradilla, D.; Bidan, G.; Gentile, P.; Weathers, P.; Thissandier, F.; Ruiz, V.; Gómez-Romero, P.; Schubert, T. J. S.; Sahin, H.; Sadki, S. Novel Hybrid Micro-Supercapacitor Based on Conducting Polymer Coated Silicon Nanowires for Electrochemical Energy Storage. *RSC Adv.* **2014**, *4*, 26462−26467.
(57) Aradilla, D.; Gaboriau, D.; Bidan, G.; Gentile, P.; Boniface, M.; Dubal, D.; Gomez-Romero, P.; Wimberg, J.; Schubert, T. J. S.; Sadki, S. An Innovative 3-D Nanoforest Heterostructure Made of Polypyrrole Coated Silicon Nanotrees for New High Performance Hybrid Micro-Supercapacitors. *J. Mater. Chem. A* **2015**, *3*, 13978−13985.

DOI: 10.1021/acscatal.5b01546
ACS Catal. 2015, 5, 6138−6147